Numerical calculation of the rate of homogeneous gas–liquid nucleation in a Lennard-Jones system

Pieter Rein ten Wolde
FOM Institute for Atomic and Molecular Physics, Kruislaan 407, 1098 SJ Amsterdam, The Netherlands

Maria J. Ruiz-Montero
Física Teórica, Facultad de Física, Apdo. de Correos 1065, 41080 Sevilla, Spain

Daan Frenkel
FOM Institute for Atomic and Molecular Physics, Kruislaan 407, 1098 SJ Amsterdam, The Netherlands

(Received 25 August 1998; accepted 14 October 1998)

We report a computer-simulation study of the absolute rate of homogeneous gas–liquid nucleation in a Lennard-Jones system. The height of the barrier has been computed using umbrella sampling, whereas the kinetic prefactor is calculated using molecular dynamics simulations. The simulations show that the nucleation process is highly diffusive. We find that the kinetic prefactor is a factor of 10 larger than predicted by classical nucleation theory. © *1999 American Institute of Physics.* [S0021-9606(99)50803-9]

I. INTRODUCTION

The formation of liquid droplets from a supersaturated vapor is an activated process. When a vapor is supersaturated, the liquid phase is more stable than the vapor. However, due to the free-energy barrier separating the two phases, the vapor will not condense immediately. First, nuclei of the new phase have to form. Two competing contributions determine the excess free energy of such nuclei. The difference in chemical potential between vapor and liquid drives the nucleation process, whereas the surface free energy frustrates the formation of nuclei. Initially, the surface free energy dominates, and hence the excess free energy of a droplet increases with size. However, beyond a certain ''critical'' nucleus size, the volume term takes over, and the excess free energy decreases. It is only from here on that a nucleus grows spontaneously into a bulk liquid.

The classical nucleation theory of homogeneous gas–liquid nucleation was formulated over half a century ago.[1,2] This theory is partly phenomenological in nature. Subsequently, various modifications and extensions have been proposed,[3–9] and much progress has been made in the development of statistical-mechanical theories of nucleation.[10–12] In parallel, nucleation rate measurements have become increasingly precise. This makes it possible to test the theoretical predictions for the nucleation rate.[13–23] However, in the experiments only the nucleation rate can be probed. It is virtually impossible to study the critical nuclei themselves. The reason is precisely that nucleation is an activated process. The rate k of such a process can be written as

$$k = C\rho_v e^{-\beta\Delta G^*} = C\rho_{n*}. \tag{1}$$

Here, C is a prefactor, $\beta \equiv 1/k_B T$ is the reciprocal temperature, with k_B Boltzmann's constant and T the absolute temperature, ρ_v is the number density of the vapor, and ΔG^* is the nucleation barrier which is given by the excess free energy of the critical nucleus. The nucleation rate is the product of two factors: (1) the density ρ_{n*} of critical nuclei and (2) the rate C at which these nuclei cross the barrier. The rate of nucleation strongly depends on the conditions. Typically, the height of the barrier is on the order of $20-60k_BT$. This implies that the density of critical nuclei is small, on the order of $10^{10}-10^{-7}/\mathrm{cm}^3$ at atmospheric pressure ($\rho_v = 10^{19}/\mathrm{cm}^3$). If we take a typical experimental nucleation rate of 10^6 nuclei formed per cubic centimeter per second,[16] and a barrier height of $50k_BT$, then the prefactor is in the gigahertz range. This means that when a nucleus reaches its critical size, it spends only little time at the top of the barrier. Hence, nucleation is both infrequent and fast and it is very difficult to study the structure and dynamics of the critical nuclei. Experiments only measure the overall nucleation rate. It is not possible to measure the factors that determine the nucleation rate independently. It is for these reasons that computer simulation is a natural complementary tool to study the nucleation process. By employing umbrella sampling[24] we can stabilize the critical nuclei, which allows us to study the structure of a nucleus and to compute its free energy as a function of its size. Moreover, using the Bennett–Chandler scheme[25–27] we can also compute the kinetic prefactor.

Gas–liquid nucleation proceeds via the addition of single particles from the vapor. This is a sequence of uncorrelated events. As a consequence, the nucleation process is diffusive, rather than ballistic. Recently, we have shown how the Bennett–Chandler scheme can be modified to study diffusive barrier crossings.[28] Here we apply this extended scheme to study gas–liquid nucleation in a Lennard-Jones system. The choice of the Lennard-Jones system as a model for a simple fluid is motivated by several factors: First of all, the phase behavior and surface tension of this system are known. This makes it possible to compare the simulation results with classical nucleation theory.[2] Second, in a previous paper, we have computed the nucleation barrier for the Lennard-Jones system.[29]

The rest of the paper is organized as follows: In Sec. II we briefly discuss the Bennett–Chandler scheme and the modifications described in Ref. 28. We then describe some technical aspects of the simulations. We end with a discussion of the results.

II. CROSSING RATE

Nucleation is an activated process and the rate limiting step in the condensation of the vapor. This implies that in order to compute the rate of nucleation, we can calculate the rate at which the vapor transforms into the liquid and vice versa. We apply the Bennett–Chandler scheme[25–27] to compute rate constants for a transition between two states, A (vapor) and B (liquid), that are separated by a free-energy barrier. In the Bennett–Chandler scheme it is assumed that the reaction can be described by a first-order phenomenological rate law:

$$\Delta P_A(t) = \Delta P_A(0) e^{-t/\tau}. \tag{2}$$

Here P_A is the probability that the system is in state A (vapor). According to the Onsager-regression hypothesis the relaxation of the macroscopic variable P_A is given by the regression of spontaneous fluctuations of a microscopic variable, n_A, in an equilibrium system:[30]

$$\Delta P_A(t)/\Delta P_A(0) \propto \langle \Delta n_A(t) \Delta n_A(0) \rangle_{\mathrm{eq}}. \tag{3}$$

Here $\Delta P_A(t)$ and $\Delta n_A(t)$ are the deviations of P_A and n_A from their equilibrium value at time t, respectively, and τ is the relaxation time. The brackets $\langle \cdots \rangle_{\mathrm{eq}}$ denote an equilibrium average.

We now have to determine the characteristic, microscopic functions, n_A and n_B, the value of which specifies whether the system is in state A (vapor) or state B (liquid). To this end, we first have to define a reaction coordinate that connects the vapor with the liquid phase. For now, let us assume that we have such a coordinate, that we denote by q_1. The transition state separating the liquid from the vapor is denoted by q_1^*. The conventional definition for the characteristic functions is

$$n_A = \theta(q_1^* - q_1), \tag{4}$$

$$n_B = \theta(q_1 - q_1^*), \tag{5}$$

where θ is the Heaviside function.

We then arrive at the following microscopic expression for the rate constant k_{AB}:[30]

$$k_{AB} = \frac{\langle \dot{q}_1 \delta(q_1 - q_1^*) \theta(q_1(t) - q_1^*) \rangle_{\mathrm{eq}}}{\langle \theta(q_1^* - q_1) \rangle_{\mathrm{eq}}} = M(t), \tag{6}$$

where δ is the Dirac delta function. The time correlation function $M(t)$ explicitly depends on time, whereas k_{AB} does not. Hence, Eq. (6) is only valid if and when $M(t)$ reaches a plateau value, after an initial transitory period.

In transition state theory (TST) it is assumed that all trajectories that have crossed the top of the free-energy barrier, proceed to the final state and do not recross the barrier to the initial state. This implies that all trajectories that initially head from the top of the barrier to a given state, will end up in that state. The crossing rate that corresponds to this situation can be obtained by taking the limit $t \to 0^+$ in the expression for the transition rate in Eq. (6):

$$\begin{aligned} k_{\mathrm{TST}} &= \lim_{t \to 0^+} M(t) \\ &= \frac{\langle |\dot{q}_1^*| \rangle_{\mathrm{eq}}}{2} \frac{\langle \delta(q_1 - q_1^*) \rangle_{\mathrm{eq}}}{\langle n_A \rangle_{\mathrm{eq}}} \\ &= \frac{\langle |\dot{q}_1^*| \rangle_{\mathrm{eq}}}{2} P_0(q_1^*). \end{aligned} \tag{7}$$

It is seen that k_{TST} is the product of two contributions. The first contribution is the average flux of trajectories over the top of the barrier, and the second contribution is the relative probability for the system to be at the top of the barrier. The probability density for the system to be at the top of the barrier, divided by the probability that it is in the vapor state is given by

$$P_0(q_1^*) = \frac{e^{-\beta F(q_1^*)}}{\int_0^{q_1^*} dq_1' e^{-\beta F(q_1')}}, \tag{8}$$

where $F(q_1)$ is the free energy of the system at the reaction coordinate q_1.

Only the trajectories that are in the initial state at time $-t$ and in the final state at time t, contribute to the transition rate. Those trajectories that recross the barrier do not contribute. It is conventional to express the reduction of k_{AB} due to recrossing in terms of the transmission coefficient κ, defined as

$$\kappa = \frac{k_{AB}}{k_{\mathrm{TST}}}. \tag{9}$$

Ruiz-Montero *et al.* derived a general expression for the rate constant by studying the response of the system to an initial perturbation.[28] They found:

$$M(t) \equiv \frac{\langle n_B \rangle_{\mathrm{eq}}}{\langle \Delta n_A \Delta \chi \rangle_{\mathrm{eq}}} \langle \dot{q}_1 \chi'(q_1) n_A(t) \rangle_{\mathrm{eq}} \tag{10}$$

$$= k_{AB}. \tag{11}$$

Here n_A and n_B are again the characteristic functions and χ is the perturbation function that specifies the initial perturbation. The Bennett–Chandler expression [Eq. (6)] is recovered by taking for both the perturbation function and the characteristic functions a step function. However, we have considerable freedom in our choice for both functions. This is important, because Eq. (6) is less useful for diffusive barrier crossings.[28]

One of the main problems is that a θ-function perturbation does not prepare the system in the steady state initially. When the initial perturbation is a step function, we increase the probability of state A and decrease the probability of state B by the same amount. The steady state, however, corresponds to a much smoother probability distribution. Hence, the system first has to relax to the steady state, a process which in the case of diffusive barrier crossings can be slow. We can eliminate this problem by initially preparing the sys-

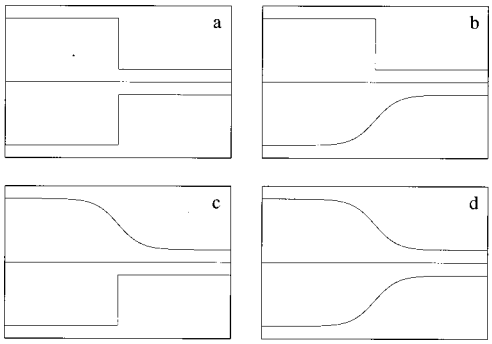

FIG. 1. Sketch of the the perturbation functions and the characteristic functions: (a)–(d) correspond to the transmission coefficients $\kappa_1-\kappa_4$, defined in Eqs. (16)–(25), respectively. The top panel shows the perturbation function $\chi(q_1)$ and the bottom panel shows the characteristic function $n_B(q_1)=1-n_A(q_1)$.

tem such that it is already close to the steady state. This can be accomplished by taking the following form for the initial perturbation function:[28]

$$\chi(q_1)=1+\epsilon(q_{1A})\left[1-\frac{\int_{q_{1A}}^{q_1}dq_1'e^{\beta F(q_1')}}{\int_{q_{1A}}^{q_{1B}}dq_1'e^{\beta F(q_1')}}\right]. \tag{12}$$

Still, we can do better. We are also free to choose other characteristic functions for n_A and n_B, as long as they only differ in the regions of configuration space that contribute negligibly to the equilibrium averages. This means that we can choose other functional forms for n_A and n_B near the top of the barrier, but not in state *A* or state *B*. We will therefore use functions that behave like the Heaviside functions in state *A* and *B*, but vary more smoothly near the top of the barrier. The advantage is that a continuous function that varies smoothly can be expected to yield much better statistics than a step function.[28] The characteristic functions are given by

$$n_A(q_1)=1-\frac{\int_{q_{1A}}^{q_1}dq_1'e^{\beta F(q_1')}}{\int_{q_{1A}}^{q_{1B}}dq_1'e^{\beta F(q_1')}} \tag{13}$$

and $n_B(q_1)=1-n_A(q_1)$.

We have computed the transmission coefficient κ in four different ways, that differ from each other in the choice for the perturbation function and the form of the characteristic function. In Fig. 1 we show the different functions. In the Appendix we give a derivation of the expressions for the transmission coefficients that we used in the simulations. Below we list the results.

(1) The conventional way of computing the transmission coefficient. Both the initial perturbation and the characteristic function are a Heaviside function:

$$\chi(q_1)=\theta(q_1^*-q_1)/\langle\theta(q_1^*-q_1)\rangle_{\rm eq}, \tag{14}$$

$$n_A(q_1)=\theta(q_1^*-q_1). \tag{15}$$

Combining Eq. (6) with Eq. (9) and using the fact that $\langle A(q_1)\delta(q_1-q_1^*)\rangle_{\rm eq}=\langle A\rangle_c\langle\delta(q_1-q_1^*)\rangle_{\rm eq}$, where the subscript *c* indicates that the average is over states constrained at the top of the barrier, we obtain the following expression for κ:

$$\kappa_1(t)=\langle\dot q_1\theta(q_1(t)-q_1^*)\rangle_c\,\frac{2}{\langle|\dot q_1^*|\rangle_{\rm eq}}. \tag{16}$$

(2) The initial perturbation is still a Heaviside function, but the characteristic function is now a function that behaves like the Heaviside function in state *A* and state *B*, but behaves more smoothly near the top of the barrier:

$$\chi(q_1)=\theta(q_1^*-q_1)/\langle\theta(q_1^*-q_1)\rangle_{\rm eq}, \tag{17}$$

$$n_A(q_1)=1-\frac{\int_{q_{1A}}^{q_1}dq_1'e^{\beta F(q_1')}}{\int_{q_{1A}}^{q_{1B}}dq_1'e^{\beta F(q_1')}}. \tag{18}$$

This yields for the transmission coefficient

$$\kappa_2(t)=\frac{\int_0^t dt'\langle\dot q_1(0)\dot q_1(t')e^{\beta F(q_1(t'))}\rangle_c}{\int_{q_{1A}}^{q_{1B}}dq_1'e^{\beta F(q_1')}}\,\frac{2}{\langle|\dot q_1^*|\rangle_{\rm eq}}. \tag{19}$$

(3) The initial perturbation is the smooth function, but the characteristic function is still the Heaviside function:

$$\chi(q_1)=1+\epsilon(q_{1A})\left[1-\frac{\int_{q_{1A}}^{q_1}dq_1'e^{\beta F(q_1')}}{\int_{q_{1A}}^{q_{1B}}dq_1'e^{\beta F(q_1')}}\right], \tag{20}$$

$$n_A(q_1)=\theta(q_1^*-q_1). \tag{21}$$

The starting points for the simulations to compute the transition rate are not states at the top of the barrier, but near the top of the barrier, obtained from a biased ensemble with weighting function *w*. The expression for the transmission coefficients is obtained by combining Eq. (A21) of the Appendix with Eq. (9):

$$\kappa_3(t)=\frac{\langle\dot q_1(0)e^{\beta F(q_1(0))}n_B(t)w^{-1}(q_1)\rangle_w}{\int_{q_{1A}}^{q_{1B}}dq_1'e^{\beta F(q_1')}}\times\frac{\langle w\rangle_{\rm eq}}{\langle\delta(q_1-q_1^*)\rangle_{\rm eq}}\,\frac{2}{\langle|\dot q_1^*|\rangle_{\rm eq}}. \tag{22}$$

(4) Both the initial perturbation and the characteristic function are smooth near the top of the barrier:

$$\chi(q_1)=1+\epsilon(q_{1A})\left[1-\frac{\int_{q_{1A}}^{q_1}dq_1'e^{\beta F(q_1')}}{\int_{q_{1A}}^{q_{1B}}dq_1'e^{\beta F(q_1')}}\right], \tag{23}$$

$$n_A(q_1)=1-\frac{\int_{q_{1A}}^{q_1}dq_1'e^{\beta F(q_1')}}{\int_{q_{1A}}^{q_{1B}}dq_1'e^{\beta F(q_1')}}. \tag{24}$$

Again the starting points for the computation of the flux are taken from a weighted ensemble. The expression for the transmission coefficient is found from Eq. (A26) of the appendix and Eq. (9):

$$\kappa_4(t)=\frac{\int_0^t dt'\langle \dot{q}_1(0)e^{\beta F(q_1(0))}\dot{q}_1(t')e^{\beta F(q_1(t'))}w^{-1}(q_1)\rangle_w}{[\int_{q_{1A}}^{q_{1B}}dq_1' e^{\beta F(q_1')}]^2}$$

$$\times\frac{\langle w\rangle_{\rm eq}}{\langle\delta(q_1-q_1^*)\rangle_{\rm eq}}\frac{2}{\langle|\dot{q}_1^*|\rangle_{\rm eq}}. \qquad (25)$$

The nucleation rate is given by $k_{AB}=\kappa k_{\rm TST}$. In order to compute $k_{\rm TST}$ we have to know the (relative) probability $P_0(q_1^*)$ of finding the system at the top of the barrier. In Ref. 29 we have used umbrella sampling[24] to calculate the free-energy barrier and hence, $P_0(q_1^*)$ [see Eq. (8)]. In the present section we simply use the result of Ref. 29 for the barrier height and use this as a starting point for the computation of the transmission coefficient. We have performed molecular dynamics simulations to calculate the transmission coefficient in the four different ways described above. The starting configurations for these calculations were obtained from an umbrella-sampling simulation near the top of the barrier. Configurations exactly at the top of the barrier, needed to compute κ_1 and κ_2, were also obtained from these simulations. We stress that our computational scheme obviates the need to perform constrained MD simulations at the top of barrier.[27]

III. DETAILS OF THE SIMULATIONS

In order to calculate the nucleation rate we have to define a reaction coordinate that monitors the progress of the transition. We have considerable freedom in our choice for the reaction coordinate. Although both the relative probability for the system to be at the top of the barrier, and the flux over the top of the barrier do depend on the choice for the reaction coordinate, the rate, which is the product of the two, does not.[28] Nevertheless, in practice it is convenient to use a local order parameter, rather than a global order parameter, such as the density of the system. The reason is that, under certain conditions, it can be entropically favorable to distribute a given amount of the new phase over many small nuclei instead of over a single large cluster.[31] In the nucleation process we are only interested in the largest liquid cluster. We therefore define the number of particles in this cluster as our reaction coordinate. To identify the particles that constitute the largest cluster, we used a geometric cluster criterion, that is derived from the one proposed by Stillinger.[32] Particles that have a significantly higher local density than the particles in the remainder of the system are identified as ''liquidlike'' particles. All liquidlike particles that are less than $q_c=1.5\sigma$ apart, are considered to be connected and, therefore, belong to the same cluster. For more details, see Ref. 29.

All MD simulations were performed in the isobaric–isothermal (*NPT*) ensemble. To control the pressure and temperature we employed the extended system method proposed by Andersen[33] and Nosé.[34] The algorithm to integrate the equations-of-motion was derived by a Trotter factorization of the Liouville operator.[35] The reversible integrator is similar to the algorithm recently developed by Martyna *et al.*[36] We used a time step of 0.01τ, where $\tau=\sqrt{\epsilon/m\sigma^2}t$ is the unit of time, with m the mass, σ the Lennard-Jones diameter, and ϵ the Lennard-Jones well depth. In what follows, we use reduced units, such that the Lennard-Jones well depth ϵ is the unit of energy and the Lennard-Jones diameter σ is the unit of length.

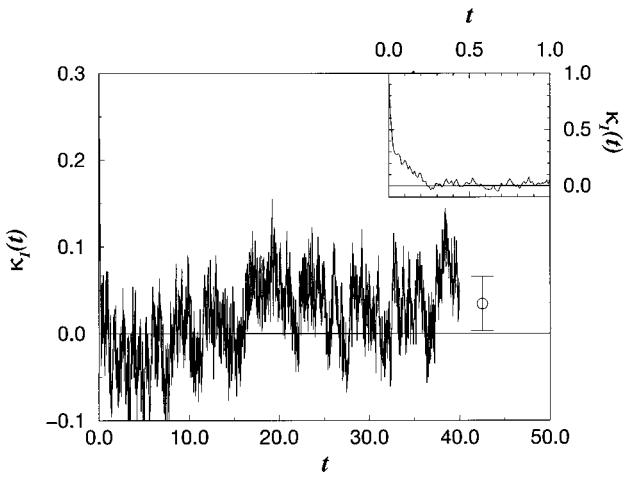

FIG. 2. Transmission coefficient as a function of time for homogeneous gas–liquid nucleation in a Lennard-Jones system at a supersaturation $S=1.53$ ($T=0.741$, $P=0.012$). The transmission coefficient is computed via Eq. (16). The plateau value $\kappa=0.03\pm0.03$. Here, and in subsequent figures, the reported estimate is based on the plateau value of k at $20<t<40$.

In order to calculate the transition rate, we performed umbrella simulations near the top of the barrier to generate a sequence of uncorrelated configurations. These configurations were used as initial states for the computation of the transmission coefficients in Eqs. (16)–(25). For every calculation we used 300 independent configurations. At the beginning of the unconstrained runs, all particles were given a velocity drawn from a Maxwell–Boltzmann distribution. Furthermore, we made use of the time-reversal property $\kappa(\tau)=-\kappa(-\tau)$. This means that every initial configuration was not only propagated forwards in time, but also backwards. Hence, the results that we present here were averaged over 600 trajectories.

We computed the rate of nucleation of the Lennard-Jones system under the conditions studied in Ref. 29. The interaction potential was truncated and shifted at a cutoff radius $r_c=2.5\sigma$, where σ is the Lennard-Jones particle diameter. We made no long-range correction and applied cubic periodic boundary conditions. The number of particles was $N=864$.

IV. RESULTS

We have calculated the transition rate for homogeneous gas–liquid nucleation in a Lennard-Jones system at $T=0.741$ and $P=0.012$, corresponding to a supersaturation $S=P/P_{\rm coex}=1.53$. Under these conditions, the barrier height is $\beta\Delta G^*=59.4\pm0.6$.[29] We computed the transmission coefficient in four different ways, according to Eqs. (16)–(25). Figures 2–5 show the results. First, we discuss the different ways of computing the transmission coefficients. Next, we make a comparison with classical nucleation theory.

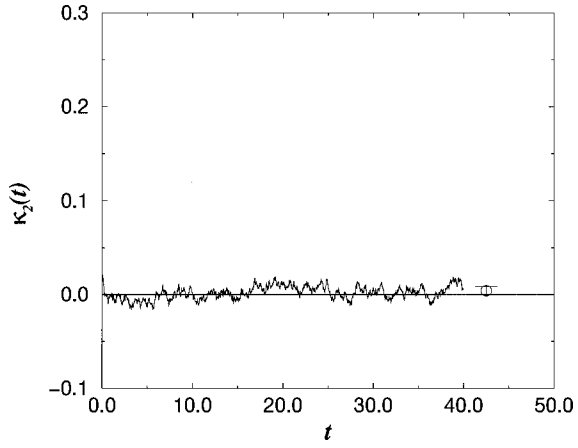

FIG. 3. Transmission coefficient as a function of time for homogeneous gas–liquid nucleation in a Lennard-Jones system at a supersaturation $S=1.53$ ($T=0.741$, $P=0.012$). The transmission coefficient is computed via Eq. (19) and is found to be $\kappa=0.004\pm0.004$.

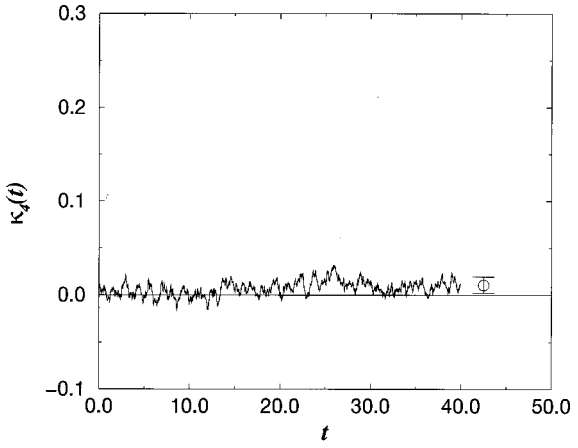

FIG. 5. Transmission coefficient as a function of time for homogeneous gas–liquid nucleation in a Lennard-Jones system at a supersaturation $S=1.53$ ($T=0.741$, $P=0.012$). The transmission coefficient is computed via Eq. (25) and is found to be $\kappa=0.011\pm0.009$.

A. Transmission coefficient: Comparison of characteristic functions and perturbation functions

Figure 2 shows the transmission coefficient, as defined in Eq. (16). Here we have computed the transmission coefficient in the conventional way: both the initial perturbation and the characteristic function are Heaviside functions. As explained, we expect that this perturbation gives rise to a transitory regime, in which the system relaxes to the steady state. Indeed, as can be seen from Fig. 2, the transmission coefficient initially drops from the value $\kappa=1$ at $t=0$. This is due to recrossings. Only after a fairly long transitory period, the transmission coefficient reaches a plateau value. It is also seen that the initial decay is very rapid and that the plateau value is very small. This indicates that the nucleation process is highly diffusive. A direct analysis of the trajectories support this view: The system stays close to the top of the barrier and does not end up in either minimum (gas or liquid one) during the run.

It is also clear from Fig. 2 that the statistical noise is large, even though averages were taken over 600 trajectories.

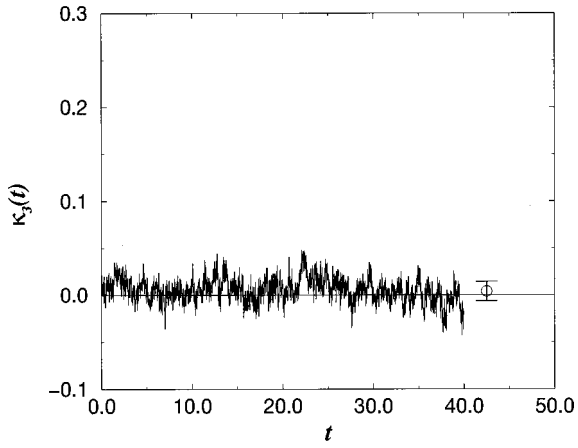

FIG. 4. Transmission coefficient as a function of time for homogenous gas–liquid nucleation in a Lennard-Jones system at a supersaturation $S=1.53$ ($T=0.741$, $P=0.012$). The transmission coefficient is computed via Eq. (22). We find $\kappa=0.004\pm0.01$.

A smoother characteristic function should increase the statistical accuracy. This is illustrated in Fig. 3. In this case the characteristic function is not the Heaviside function, but the function in Eq. (18). This function behaves like the Heaviside function in the vapor and liquid state, but changes more smoothly near the top of the barrier. We found that this choice of the characteristic function decreases the error bar by a factor of 7.

However, the drawback is that we have not prepared the system close to the steady state situation. For diffusive barrier crossings, the approach to the stationary state can be slow. Moreover, it is conceivable that the transmission coefficient *appears* to have reached a plateau value, but that in fact, it has not, due to the slow dynamics at the top of the barrier. It is therefore advisable to prepare the system close to the steady state. To this end, we choose as the initial perturbation not a step function, but the function given in Eq. (20). The result is shown in Fig. 4. We see that the transient regime is suppressed and that the transmission coefficient reaches its plateau value immediately. This shows that indeed the system is already close to the steady-state situation initially.

In Fig. 5 we show the transmission coefficient computed via Eq. (25). Now both the initial perturbation and the characteristic function are Heaviside-like functions that, however, vary continuously near the top of the barrier. We see that in comparison with Fig. 4 the error bar is slightly reduced and we use the value for κ_4 to estimate the nucleation rate. We find $\kappa_4=0.011\tau^{-1}\pm0.009\tau^{-1}$. This estimate is based on the plateau value of κ_4 at $20<t<40$. However, κ_4 appears to approach a constant value much sooner. This allows us to discard the long-time data that contribute little to the signal, but much to the noise. If we compute the plateau value of κ_4 for $2.5<t<10$, we find $\kappa_4=0.002\pm0.004$. At first sight this is a disappointing result: The error in the transmission coefficient is 100%. However, we know that κ must be positive. Moreover, we stress that an error of one $\kappa_B T$ in the calculation of the barrier height leads to a larger error in the estimate of the nucleation rate. Still, in order to obtain a

better estimate for the transmission coefficient, we performed additional simulations to determine κ_4. To this end we extracted 200 extra configurations from the umbrella-sampling simulation near the top of the barrier. Furthermore, we used every starting configuration not once (or actually twice as every configuration is propagated backwards and forwards in time), but ten times (or twenty times), by assigning different initial velocities to the same configuration. We thus averaged over 10 000 trajectories. The result is $\kappa_4 = 0.003 \pm 0.002$, which is close to the previous result. Although the error in the transmission coefficient is still nearly 100%, it is much smaller than can be obtained with any other technique and, to our knowledge, much smaller than the error in any other computed transmission coefficient reported in the literature. Another test to verify if the result that we obtain is of the correct order of magnitude, is to fit the very short-time behavior of the correlation function in Eq. (25) to an exponential. Although the fit to an exponential is less than perfect (the actual correlation function decays faster), its integral is again of the same order of magnitude ($\kappa_4 = 0.013 \pm 0.002$).

To obtain the full nucleation rate, we can combine the value of the transmission coefficient with the prediction of transition-state theory (TST) for the crossing rate [see Eq. (9)]. The TST prediction is the product of the average probability for the system to be at top of the barrier and the rate at which this barrier is crossed. From the measured nucleation barrier (see Ref. 29) we find via Eq. (8) that the relative probability for the system to be at the top of the barrier is $P_0 = 1.63 \times 10^{-26}$. The average of the absolute value of the velocity of the order parameter at the top of the barrier is $\langle |\dot{q}_1| \rangle = 76.2 \tau^{-1}$. Hence, the rate in the transition-state theory approximation is $k_{\mathrm{TST}} = 6.2 \times 10^{-25} \tau^{-1}$. From k_{TST} and the transmission coefficient we get the full nucleation rate $k_{AB} = k_{\mathrm{TST}} \kappa = 1.8 \times 10^{-27} \tau^{-1}$.

The rates found from our simulations are measured in number of nuclei per unit time. Experimental nucleation rates are often expressed as the number of nuclei formed per unit volume per unit time. To obtain such a quantity we note that

$$k = \kappa k_{\mathrm{TST}} = C_s \frac{\langle \delta(q - q_1^*) \rangle_{\mathrm{eq}}}{\langle n_A \rangle_{\mathrm{eq}}} \tag{26}$$

$$= C_s \frac{N(n^*)}{\sum_{n=0}^{n=n^*} N(n)}, \tag{27}$$

$$= C_s \frac{e^{-\beta \Delta G(n^*)}}{\sum_{n=0}^{n=n^*} e^{-\beta \Delta G(n)}}. \tag{28}$$

Here N is the total number of particles, $N(n)$ is the number of nuclei of size n, and we have used that $\beta \Delta G(n) \equiv -\ln[N(n)/N]$. Note that the kinetic prefactor is given by $C_s = \kappa \langle |\dot{q}_1| \rangle_{\mathrm{eq}}/2$. If we now multiply the above expression with $\rho_v \sum_{n=0}^{n=n^*} e^{-\beta \Delta G(n)}$, where ρ_v is the density in the vapor, we find

$$k = C_s \rho_v e^{-\beta \Delta G(n^*)}. \tag{29}$$

This expression for the nucleation rate yields the number of liquid particles produced per unit volume per unit time. It can be interpreted as the number density of nuclei at the top of the barrier, multiplied with the net rate C_s at which these nuclei gain particles. We find from the simulations that $C_s = 0.11 \pm 0.08 \tau^{-1}$, $\rho_v = 0.0188 \pm 0.0005 \sigma^{-3}$, and $\beta \Delta G(n^*) = 59.4 \pm 0.6$. Hence, we finally obtain for the rate of nucleation $k = 3.5 \times 10^{-29} \sigma^{-3} \tau^{-1}$.

TABLE I. Nucleation rates k_{AB} for a number of apolar compounds, as deduced from the simulations. The values for ϵ and σ are taken from Ref. 37. In order to facilitate a comparison with experiments we also give the temperatures T (in kelvin) and pressures P (in kPa).

Compound	k_{AB} ($\mathrm{cm}^{-3}\,\mathrm{s}^{-1}$)	T (K)	P (kPa)
Ar	4.05e+05	88.88	503
Kr	2.68e+05	127	607
N2	3.09e+05	70.5	311
CH4	4.50e+05	110	442
CF4	8.49e+04	113	243
CCl4	3.84e+04	242	266
SF6	4.00e+04	149	199

To our knowledge, there is a scarcity of quantitative data on nucleation in spherical, nonpolar fluids, such as argon. However, in order to facilitate a future comparison of our data with experimental data, we have converted the rate constant to experimental units, i.e., units of number of nuclei formed per cubic centimeter per second. We have done this for a variety of compounds that obey the principle of corresponding states. Table I shows the results. It is interesting to note that in recent experiments by Strey *et al.* on a variety of compounds,[16–20] the measured nucleation rates were of the same order of magnitude. This illustrates that it is indeed possible to use simulation to predict nucleation rates under conditions that are typical of real experiments.

B. Comparison with classical nucleation theory

In classical nucleation theory (CNT), the rate of nucleation is given by[38]

$$k_{\mathrm{CNT}} = Z f_e(n^*) \rho(1) e^{-\beta \Delta G(n^*)}. \tag{30}$$

It is seen that the rate is the product of three factors.

(1) $\rho(1) e^{-\beta \Delta G(n^*)}$, where $\rho(1)$ is the number density of monomers in the supersaturated vapor and $\Delta G(n^*)$ is the height of the nucleation barrier. $\rho(1) e^{-\beta \Delta G(n^*)}$ is the concentration of nuclei that have reached the critical size. In classical nucleation theory the height of the nucleation barrier is given by

$$\Delta G^* = \frac{16 \pi \gamma^3}{3 \rho_l^2 \Delta \mu^2}, \tag{31}$$

where γ is the surface tension of a planar interface, ρ_l is the density of a bulk liquid (which is assumed to be incompressible), and $\Delta \mu$ is the difference in chemical potential between the bulk vapor and the bulk liquid, both at the supersaturation pressure P in the vapor phase

$$\Delta \mu = \mu_v(P) - \mu_l(P). \tag{32}$$

The CNT prediction for the size of the critical nucleus is

$$n^* = \frac{32\pi\gamma^3}{3\rho_l^2\Delta\mu^3}. \tag{33}$$

In Ref. 29 we compared the measured barrier height and critical nucleus size with the corresponding predictions of classical nucleation theory for various values of the supersaturation. We found that the classical nucleation theory predicts the size of the critical nuclei surprisingly well ($n^*_{\mathrm{CNT}} = 338$ compared to $n^*_{\mathrm{sim}} = 336$), and that the difference between the actual barrier height and the CNT prediction is independent of supersaturation. For $T = 0.741$ the barrier height found in the simulations differs by a constant offset of $5k_BT$ from the value predicted by CNT.

(2) $f_e(n^*)$. $f_e(n)$ is, at coexistence, the forward rate at which a cluster of size n grows by one monomer; $f_e(n^*)$ is the rate at which critical nuclei cross the barrier. The rate at which particles impinge on the surface of a nucleus of size n is given by

$$f_e(n) = A(n) q n_{1,e} \langle |v| \rangle / 4. \tag{34}$$

Here $A(n)$ is the surface area of the nucleus, q is the condensation coefficient, which is the fraction of monomers hitting the surface that actually stick, $n_{1,e}$ is the monomer density at coexistence, and $\langle |v| \rangle$ is the mean molecular speed. If we assume that the gas is ideal, then the monomer concentration at the saturation (coexistence) pressure P_e is reduced from its value $\rho(1)$ at the supersaturation pressure P by a factor $S = P/P_e$, i.e., $n_{1,e} = \rho(1)/S$. For an ideal gas, the mean velocity is

$$\langle |v| \rangle = \sqrt{\frac{8k_BT}{\pi m_1}}, \tag{35}$$

where m_1 is the mass of monomers. Furthermore, in classical nucleation theory it is assumed that the nuclei are spherical, yielding for the surface area:

$$A(n) = \left(\frac{36\pi}{\rho_l^2}\right)^{1/3} n^{2/3}. \tag{36}$$

Combining the above equations yields for the forward rate $f_e(n^*)$,

$$f_e(n^*) = A(n^*) q (\rho(1)/S) \sqrt{k_BT/2\pi m_1}. \tag{37}$$

(3) Z, the Zeldovich factor, which relates the number of critical nuclei in the equilibrium distribution to the number of critical nuclei in the steady-state distribution. It is given by

$$Z = \sqrt{Q/2\pi k_BT}, \tag{38}$$

where

$$Q \equiv -\left[\frac{\partial^2 \Delta G}{\partial n^2}\right]_{n^*} \tag{39}$$

is the second derivative of the free energy with respect to cluster size n at the top of the barrier. Using the expression of classical nucleation theory for ΔG we get

$$Z = \sqrt{\frac{\Delta\mu}{6\pi k_BTn^*}}. \tag{40}$$

The Zeldovich factor takes into account that not all nuclei that have reached the top actually cross it and end up in the liquid state. We find that $Z = 0.0066$. The low value of the Zeldovich factor reflects the fact that the barrier crossing is a diffusive rather than a ballistic process. It is this diffusive behavior which leads to recrossing and to a reduction of the transmission coefficient $\kappa(t)$.

Using the above expressions for f_e and Z we obtain for k_{CNT}

$$k_{\mathrm{CNT}} = \sqrt{\frac{2\gamma}{\pi m_1}} \frac{q\rho(1)}{S\rho_l} \rho(1) e^{-\beta\Delta G(n^*)}$$

$$\equiv C_{\mathrm{CNT}} \rho(1) e^{-\beta\Delta G(n^*)}, \tag{41}$$

where C_{CNT} is the kinetic prefactor. The number density of monomers can be well approximated by the total number density ρ_v. Hence, in order to compare the kinetic prefactor of classical nucleation theory with the kinetic prefactor as obtained from the simulations, we should compare C_{CNT} and C_s, as defined in Eq. (26). The surface tension for the planar interface is $\gamma = 0.494\epsilon\sigma^{-2}$ and the density of the bulk liquid is $\rho_l = 0.766\sigma^{-3}$.[29] The density in the vapor is $\rho_v = 0.0188\sigma^{-3}$ and the supersaturation $S = 1.53$. Furthermore, we assume that the sticking coefficient is one. Hence, the prediction of CNT for the kinetic prefactor is $C_{\mathrm{CNT}} = 0.009\tau^{-1}$. The simulations yielded $C_{\mathrm{sim}} = 0.11 \pm 0.08\tau^{-1}$. Considering the magnitude of the error in the simulation result, we can only make an order of magnitude comparison with the prediction of CNT. We find that the measured kinetic prefactor is about a factor of 10 larger than predicted by CNT. An explanation could be that the actual area of the droplet is larger than the area of a sphere with the same number of particles as in the droplet. CNT also assumes that the critical nucleus grows by uncorrelated collisions of ''freely'' moving gas particles with the cluster. It is likely that the overall impingement rate of gas monomers is larger because of the attraction of the vapor particles by the cluster.

V. CONCLUSIONS

In Ref. 29 we have computed the free-energy barrier for homogeneous gas–liquid nucleation in a Lennard-Jones system. In the present study, we focus on the dynamics of the barrier crossing in this system. We find that the nucleation process is diffusive, rather than ballistic. As a result, recrossing is significant and the transmission coefficient κ is very low, $\kappa = 0.003 \pm 0.002$. We have compared the measured kinetic prefactor with the prediction of classical nucleation theory. We find that the prefactor as obtained from the simulations is about an order of magnitude larger than the theoretical prediction. In order to facilitate a future comparison of our data with experimental data, we have converted the computed rate constant from reduced units to experimental units for a variety of compounds that obey the principle of corresponding states.

ACKNOWLEDGMENTS

This work was supported in part by ''Scheikundig Onderzoek Nederland'' (SON) with financial aid from NWO (''Nederlandse Organisatie voor Wetenschappelijk Onderzoek''). The work of the FOM Institute is part of the research program of ''Stichting Fundamenteel Onderzoek der Materie'' (FOM) and is supported by NWO.

APPENDIX: TRANSMISSION RATES FOR DIFFUSIVE BARRIER CROSSINGS

To compute the transition rate, we study the response of the system to an, as yet unspecified, perturbation. We first define the response function $\phi(t)$:

$$\phi(t)\equiv\frac{\Delta P_A(t)}{\Delta P_A(0)}, \tag{A1}$$

where $\Delta P_A(t)$ is the deviation of $P_A(t)=\langle n_A(t)\rangle$, which is the probability of finding the system in state A at time t, from its equilibrium value,

$$\Delta P_A(t)=P_A(t)-P_{A,\mathrm{eq}}=\langle\Delta n_A(t)\rangle, \tag{A2}$$

with

$$\Delta n_A=n_A-\langle n_A\rangle_{\mathrm{eq}}. \tag{A3}$$

We now impose a perturbation, denoted by the perturbation function $\chi(q_1)$, such that the initial distribution function $\rho(\mathbf{q}(0);\mathbf{p}(0))$ [with $\mathbf{q}(0)$ and $\mathbf{p}(0)$ the phase space coordinates at $t=0$] is of the form

$$\rho(q(0),p(0))=\rho_{\mathrm{eq}}\chi(q_1). \tag{A4}$$

The response of the system is then given by[28]

$$\phi(t)=\frac{\langle\Delta n_A(0)\Delta\chi(t)\rangle_{\mathrm{eq}}}{\langle\Delta n_A\Delta\chi\rangle_{\mathrm{eq}}}. \tag{A5}$$

Its time derivative is

$$\frac{d\phi}{dt}=-\frac{\langle\dot q_1\chi'(q_1)n_A(t)\rangle_{\mathrm{eq}}}{\langle\Delta n_A\Delta\chi\rangle_{\mathrm{eq}}}. \tag{A6}$$

If we assume that the relaxation is exponential, i.e.,

$$\phi(t)=e^{-t/\tau}, \tag{A7}$$

we find

$$\frac{1}{\tau}e^{-t/\tau}=\frac{\langle\dot q_1\chi'(q_1)n_A(t)\rangle_{\mathrm{eq}}}{\langle\Delta n_A\Delta\chi\rangle_{\mathrm{eq}}}. \tag{A8}$$

If we are in a time regime $t\ll\tau$, we have

$$\tau^{-1}=\frac{\langle\dot q_1\chi'(q_1)n_A(t)\rangle_{\mathrm{eq}}}{\langle\Delta n_A\Delta\chi\rangle_{\mathrm{eq}}}=\frac{k_{AB}}{\langle n_B\rangle_{\mathrm{eq}}}, \tag{A9}$$

where k_{AB} is the rate constant. This leads to the following microscopic expression for k_{AB}:

$$M(t)\equiv\frac{\langle n_B\rangle_{\mathrm{eq}}}{\langle\Delta n_A\Delta\chi\rangle_{\mathrm{eq}}}\langle\dot q_1\chi'(q_1)n_A(t)\rangle_{\mathrm{eq}} \tag{A10}$$

$$=k_{AB}. \tag{A11}$$

The time correlation function $M(t)$ explicitly depends on time, whereas k_{AB} does not. Hence, the above equation is only valid if and when $M(t)$ reaches a plateau value, after an initial transitory period.

We can now make several choices for both the initial perturbation and the characteristic function. First, we take for the characteristic function $n_A(q_1)=\theta(q_1^*-q_1)$ and for the perturbation $\chi(q_1)$,

$$\chi(q_1)=\alpha n_A(q_1), \tag{A12}$$

where $\alpha=1/\langle n_A\rangle_{\mathrm{eq}}$, which follows from the normalization condition. From this we obtain

$$k_{AB}=\frac{\langle\dot q_1 n_B'n_B(t)\rangle}{\langle n_A\rangle_{\mathrm{eq}}}\equiv M(t). \tag{A13}$$

As the characteristic function is a Heaviside function, we arrive at the following expression for the rate:

$$k_{AB}=\frac{\langle\dot q_1\delta(q_1-q_1^*)\theta(q_1(t)-q_1^*)\rangle_{\mathrm{eq}}}{\langle n_A\rangle_{\mathrm{eq}}}\equiv M(t). \tag{A14}$$

We will now impose a different initial perturbation. Following Ref. 28, we write the initial perturbation as

$$\rho(q_1)=\rho_{\mathrm{eq}}[1+\epsilon(q_1)], \tag{A15}$$

which means that $\chi=1+\epsilon(q_1)$. When the system is in the steady state, $\epsilon(q_1)$ is given by[28]

$$\epsilon(q_1)=\epsilon(q_{1A})\left[1-\frac{\int_{q_{1A}}^{q_1}dq_1'e^{\beta F(q_1')}}{\int_{q_{1A}}^{q_{1B}}dq_1'e^{\beta F(q_1')}}\right]. \tag{A16}$$

Here q_{1A} and q_{1B} are the values of the reaction coordinate in the states A and B, respectively. If we impose this perturbation, we will increase the rate at which the system reaches the steady state.

From Eq. (A10) it follows that the rate is given by

$$k_{AB}=\frac{1}{\epsilon(q_{1A})\langle n_A\rangle_{\mathrm{eq}}}\langle\dot q_1(0)\epsilon'(q_1(0))n_A(t)\rangle_{\mathrm{eq}}, \tag{A17}$$

where we have used that $n_A(q_1)\approx\epsilon(q_1)/\epsilon(q_{1A})$, and $\langle\Delta n_A\Delta n_A\rangle_{\mathrm{eq}}=\langle n_A\rangle_{\mathrm{eq}}\langle n_B\rangle_{\mathrm{eq}}$. We can obtain the derivative of $\epsilon(q_1)$ from Eq. (A16). Furthermore, noticing that $n_B(t)=1-n_A(t)$ and that $\langle\dot q_1(0)\epsilon'(q_1(0))\rangle=0$, we find for the rate:

$$k_{AB}=\frac{\langle\dot q_1(0)e^{\beta F(q_1(0))}n_B(t)\rangle_{\mathrm{eq}}}{\int_{q_{1A}}^{q_{1B}}dq_1'e^{\beta F(q_1')}\langle n_A\rangle_{\mathrm{eq}}}. \tag{A18}$$

As pointed out in Ref. 28, this average can be understood as a biased average, in which the constraining term is not a delta function, but a function that has the width of the barrier. If we take the starting points from the ensemble with a biasing function $e^{\beta F(q_1)}$, then all points will be distributed almost uniformly over the entire range of q_1, as the biasing function will exactly compensate the effect of the free-energy barrier. We do not always know the precise shape of the barrier. However, this is not really important, because the main contribution to the average comes from simulations starting in the barrier region. We therefore impose a biasing

potential that ensures that the initial points are near the top of the barrier. In Ref. 28 the optimal choice for the biasing potential is discussed in some detail. We have taken our biasing potential to be a harmonic function

$$W(q_1)=\tfrac{1}{2}k(q_1-q_1^*)^2. \tag{A19}$$

We now have to correct for the biasing. We note that, in general, the average of a quantity A in the original, equilibrium ensemble, is related to the average $\langle A\rangle_w$ in the weighted ensemble, via

$$\langle A\rangle_{\rm eq}=\frac{\langle Aw^{-1}\rangle_w}{\langle w^{-1}\rangle_w}=\langle Aw^{-1}\rangle_w\langle w\rangle_{\rm eq}, \tag{A20}$$

where w is the weighting function, which, in this case is $w(q_1)=e^{-\beta W(q_1)}$. Hence, the average in Eq. (A18) becomes

$$k_{AB}=\frac{\langle \dot q_1(0)e^{\beta F(q_1(0))}n_B(t)w^{-1}(q_1)\rangle_w}{\int_{q_{1A}}^{q_{1B}}dq_1'e^{\beta F(q_1')}\langle n_A\rangle_{\rm eq}}\langle w\rangle_{\rm eq}. \tag{A21}$$

We note that, when we know the shape of the barrier, the average of w in the equilibrium ensemble can easily be obtained via

$$\langle w\rangle_{\rm eq}=\frac{\int_{q_{1A}}^{q_{1B}}dq_1'w(q_1)e^{-\beta F(q_1')}}{\int_{q_{1A}}^{q_{1B}}dq_1'e^{-\beta F(q_1')}}. \tag{A22}$$

The advantage of the above biasing potential is that we shorten the transitory period. However, we can also improve the statistics in the steady-state regime. This can be accomplished by using a different form for the characteristic functions n_A and n_B. Instead of using Heaviside functions, we take

$$n_A(q_1)=\frac{\epsilon(q_1)}{\epsilon(q_{1A})}. \tag{A23}$$

Again, $n_B(q_1)=1-n_A(q_1)$, which gives

$$n_B(q_1)=\frac{\int_{dq_{1A}}^{dq_1}dq_1'e^{\beta F(q_1)}}{\int_{q_{1A}}^{q_{1B}}dq_1'e^{\beta F(q_1)}}. \tag{A24}$$

As discussed in Ref. 29, n_A and n_B behave in much the same way as before, except for the barrier region, where it varies rapidly. That is, in region A $n_A\approx 1$, whereas in region B $n_A\approx 0$. However, we now measure a continuous function that varies smoothly, instead of counting ''ones and zeros.'' This yields better statistics.

We can substitute the expression for n_B in Eq. (A24) into Eq. (A21). However, as the average of $\langle \dot q_1(0)e^{\beta F(q_1(0))}n_B(0)w^{-1}(q_1)\rangle_w$ vanishes, we only have to consider the change in n_B during time t:

$$n_B(t)-n_B(0)=\int_0^t dt'\dot q_1(t')\,\frac{\partial n_B(q_1(t'))}{\partial q_1}$$
$$=\frac{\int_0^t dt'\dot q_1(t')e^{\beta F(q_1(t'))}}{\int_{q_{1A}}^{q_{1B}}dq_1'e^{\beta F(q_1)}}. \tag{A25}$$

We then finally arrive at the following expression for the rate

$$k_{AB}=\frac{\int_0^t dt'\langle \dot q_1(0)e^{\beta F(q_1(0))}\dot q_1(t')e^{\beta F(q_1(t'))}w^{-1}(q_1)\rangle_w}{[\int_{q_{1A}}^{q_{1B}}dq_1'e^{\beta F(q_1')}]^2\langle n_A\rangle_{\rm eq}}$$
$$\times\langle w\rangle_{\rm eq}. \tag{A26}$$

[1] M. Volmer and A. Weber, Z. Phys. Chem., Stoechiom. Verwandtschaftsl. **119**, 277 (1926).
[2] R. Becker and W. Döring, Ann. Phys. (Leipzig) **24**, 719 (1935).
[3] J. Lothe and G. M. Pound, J. Chem. Phys. **36**, 2080 (1962).
[4] M. E. Fisher, Physics (Long Island City, NY) **3**, 255 (1967).
[5] H. Reiss, J. L. Katz, and E. R. Cohen, J. Stat. Phys. **2**, 83 (1968).
[6] A. Dillmann and G. E. A. Meier, Chem. Phys. Lett. **89**, 71 (1989).
[7] S. L. Girschick, J. Chem. Phys. **94**, 826 (1991).
[8] V. I. Kalikmanov and M. E. H. van Dongen, Europhys. Lett. **21**, 645 (1993).
[9] G. Wilemski, J. Chem. Phys. **103**, 1119 (1995).
[10] D. W. Oxtoby and R. Evans, J. Chem. Phys. **89**, 7521 (1988).
[11] K. J. Oh, X. C. Zeng, and H. Reiss, J. Chem. Phys. **107**, 1242 (1997).
[12] H. Reiss, W. K. Kegel, and J. L. Katz, Phys. Rev. Lett. **78**, 4506 (1997).
[13] J. L. Katz, J. Chem. Phys. **52**, 4733 (1970).
[14] D. Wright, R. Caldwell, C. Moxeley, and M. S. El-Shall, J. Chem. Phys. **98**, 3356 (1993).
[15] D. Wright and M. S. El-Shall, J. Chem. Phys. **98**, 3369 (1993).
[16] Y. Viisanen, R. Strey, and H. Reiss, J. Chem. Phys. **99**, 4680 (1993).
[17] R. Strey and Y. Viisanen, J. Chem. Phys. **99**, 4693 (1993).
[18] Y. Viisanen, R. Strey, A. Laaksonen, and M. Kulmala, J. Chem. Phys. **100**, 6062 (1994).
[19] R. Strey, Y. Viisanen, and P. E. Wagner, J. Chem. Phys. **103**, 4333 (1995).
[20] Y. Viisanen, P. E. Wagner, and R. Strey, J. Chem. Phys. **108**, 4257 (1998).
[21] K. N. H. Looijmans, C. C. M. Luijten, G. C. J. Hofmans, and M. E. W. van Dongen, J. Chem. Phys. **102**, 4531 (1995).
[22] K. N. H. Looijmans, C. C. M. Luijten, and M. E. W. van Dongen, J. Chem. Phys. **103**, 1714 (1995).
[23] M. M. Rudek, J. A. Fisk, V. M. Chakarov, and J. L. Katz, J. Chem. Phys. **105**, 4707 (1996).
[24] G. M. Torrie and J. P. Valleau, Chem. Phys. Lett. **28**, 578 (1974).
[25] C. H. Bennett, in *Algorithms for Chemical Computations*, edited by R. E. Christofferson (American Chemical Society, Washington, DC, 1977).
[26] D. Chandler, J. Chem. Phys. **68**, 2959 (1978).
[27] E. A. Carter, G. Ciccotti, J. T. Hynes, and R. Kapral, Chem. Phys. Lett. **156**, 472 (1989).
[28] M. J. Ruiz-Montero, D. Frenkel, and J. J. Brey, Mol. Phys. **90**, 925 (1990).
[29] P. R. ten Wolde and D. Frenkel, J. Chem. Phys. **109**, 9901 (1998).
[30] D. Chandler, *Introduction to Modern Statistical Mechanics* (Oxford University Press, New York, 1987).
[31] P. R. ten Wolde, M. J. Ruiz-Montero, and D. Frenkel, Faraday Discuss. **104**, 93 (1996).
[32] F. H. Stillinger, J. Chem. Phys. **38**, 1486 (1963).
[33] H. C. Andersen, J. Chem. Phys. **72**, 2384 (1980).
[34] S. Nosé, J. Chem. Phys. **81**, 511 (1984).
[35] M. Tuckerman, B. J. Berne, and G. J. Martyna, J. Chem. Phys. **97**, 1990 (1992).
[36] G. J. Martyna, M. E. Tuckermann, D. J. Tobias, and M. L. Klein, Mol. Phys. **87**, 1117 (1996).
[37] J. O. Hirschfelder, C. F. Curtiss, and R. B. Bird, *Molecular Theory of Gases and Liquids* (Wiley, New York, 1954).
[38] D. W. Oxtoby, J. Phys.: Condens. Matter **4**, 7627 (1992).